American Mineralogist, Volume 79, pages 316–331, 1994

Ideal associated solutions: Application to the system albite-quartz-H_2O

SHAOXIONG WEN, HANNA NEKVASIL
Center for High Pressure Research and Department of Earth and Space Sciences, State University of New York, Stony Brook, New York 11794-2100, U.S.A.

ABSTRACT

The theory of associated solutions provides a simple but rigorous framework for the use of speciation reactions to model nonideal mixing behavior of silicate melt components. Application of the theory to the system Ab-Qz-H_2O requires only *P-T* solidus data in the anhydrous and H_2O-saturated systems Ab-H_2O and Ab-Qz-H_2O to calibrate equilibrium constants of proposed modeling reactions. Because compositional data are not used in the calibration, agreement between predicted eutectic compositions and experimental data is a critical means of testing proposed model reactions. Investigation of the systems Ab-H_2O and Ab-Qz-H_2O indicates that if a modeling reaction producing a sodium silicate species is considered, neither interaction between albite and silica melt to produce new complexes nor nonideal mixing of species is required and agreement between predicted and experimental eutectic compositions can be obtained by considering only disproportionation in albite melts. The thermodynamic consequence of these assumptions is that the Ab and Qz melt components mix ideally, in agreement with available calorimetric data and in contrast with the results of Burnham and Nekvasil (1986). Use of alternate reactions (e.g., a jadeite-producing reaction) results in more complex mixing relations and discordant predicted compositions.

INTRODUCTION

Experimental phase equilibrium studies have yielded a large data base of crystal-melt equilibria. Numerous efforts have been made to systematize the available experimental results under the umbrella of a rigorous formalism with predictive capabilities such as chemical thermodynamics. Although significant progress has been made on the development of thermodynamic models for geologically relevant solid solutions, less progress has been made on modeling the behavior of silicate liquids.

Most thermodynamic modeling of silicate liquids is based predominantly on phase equilibrium constraints rather than on thermochemical data because of the greater abundance of the former. Phase equilibrium data can be used on a multicomponent basis, in which data are regressed simultaneously for interaction parameters. In this case, however, unless data in the compositionally simpler subsystems are also used in the regression, the Margules parameters obtained may be inconsistent with such data and may contain little information about the energetics of interaction of specific components. It is likely therefore that such parameters will have only poor predictive capabilities in the compositional space beyond the compositions used in their calibration.

Thermodynamic modeling of silicate liquids can also be approached by successively evaluating simple systems in order to systematize the effects of each compositional variable and then using the resulting models to predict phase equilibria in higher order systems. This approach enhances our understanding of the controls on phase equilibria and maintains internal consistency with data in both simple and multicomponent systems. Margules formalism has been the traditional basic tool for describing the mixing behavior of silicate melt components; however, an alternative approach in the form of associated solution theory has been used by chemists, metallurgists, and material scientists to model the thermodynamic mixing properties of a wide variety of nonelectrolyte solutions, ranging from molten metals (e.g., Chuang and Chang, 1982) to silicate slags (e.g., Barry et al., 1993). This approach, first discussed in detail through its application to liquid organic mixtures by Dolazalek (1908) and to liquid alloys by Hildebrand and Eastman (1915), has become increasingly popular in metallurgy and slag research (e.g., Barry et al., 1993) as a conceptually simple means of modeling even complex nonideal behavior in liquids. The general approach is to begin in the unary systems and build up to the binaries and, if necessary, to the ternary systems, with the expectation that assessment of higher order behavior can be done on a predictive basis. This predictive capability has been realized in numerous slag and metallurgical systems. In addition to the simplicity of the theory and the conceptual ease with which it can be extrapolated to more complex systems, one of its most important capabilities is that it provides a framework whereby microscopic information (e.g., spectroscopic data) can be used in the development of thermodynamic mixing models.

The theory of associated solutions has thus far been applied to geologic systems only a limited extent. Shaw (1968), Stolper (1982), and Silver and Stolper (1985, 1989) used melt speciation reactions to model the thermody-

0003–004X/94/0304–0316$02.00

namic behavior of H_2O-bearing silicate melts and thus incorporated many of the elements of associated solution theory. By viewing silicate melt component interactions as a result of the production of new melt species, Burnham (1981) also used some of the fundamentals of associated solution theory (although only on a qualitative basis, since he did not use proposed reactions to constrain activity-composition relations quantitatively) in the system Ab-An-Or-Qz-H_2O. Burnham and Nekvasil (1986) likewise used speciation reactions to constrain activity-composition relations in this system. However, by not formulating equilibrium constants, they were unable to maintain thermodynamic consistency throughout this compositional space. As discussed below, many of the problems that they encountered were a result not of the concept of speciation itself but of the failure to adhere strictly to associated solution theory.

Associated solutions

Associated mixtures, as defined by Marcus (1977, p. 183), are those in which there is chemical evidence (preferably non-thermodynamic, such as spectroscopic) for the dissociation of at least one of the components, association of at least one of the components with itself (self-association), or interaction between two or more components to produce new associated complexes (or species: Prigogene and Defay, 1954, p. 411). Association may be treated in terms of one or more definite chemical reactions to which one or more equilibrium constants may be assigned and standard changes of thermodynamic quantities obtained. If the species are treated as ideal, the mixture is an ideal associated solution; otherwise the solution may be considered a regular associated solution. Although spectroscopic information is desirable to indicate the nature of the associated complexes, the choice of these complexes can be made by inference and tested by their usefulness in modeling by their ability to predict phase equilibria accurately.

When considering associated solutions it is necessary to distinguish between the nominal and actual composition of the mixture. The former is given in terms of the components that can be independently added to form the mixture (components in the thermodynamic sense; e.g., C and O in the system C-O) the actual composition of the mixture is given by the identity and abundances of the real chemical constituents, that is, the chemical species that are formed by association or dissociation, as well as the unassociated species (e.g., C, CO, CO_2, O_2). Distinguishing between the thermodynamic properties of the species and the components is crucial for rigorous application of the theory yet is a ready source of confusion. Therefore, some of the basic relations are summarized below.

On the simplest level, one can consider an associated mixture of components B and D consisting of chemical species b (nominal component B), d (nominal component D), and one or more species b_id_j. The number of moles of component B is given by

$$n_B = n_b + \sum_i i \cdot n_{b_id_j}$$

and similarly for component D. The number of moles of the unassociated species b is therefore

$$n_b = n_B - \sum_i i \cdot n_{b_id_j} \quad (1)$$

The chemical potentials μ_B and μ_D of the nominal melt components can be readily related to those of the corresponding unassociated molecular species b and d. If the homogeneous melt reaction $ib + jd = b_id_j$ is considered, then $\mu b_id_j = i\mu_b + j\mu_d$, and from the total change in Gibbs free energy at constant T and P and Equation 1 above

$$\begin{aligned} dG^{liq} &= \mu_b dn_b + \mu_d dn_d + \sum_{i,j} \mu_{b_id_j} dn_{b_id_j} \\ &= \mu_b dn_b + \mu_d dn_d + \mu_b \sum_{i,j} i \cdot dn_{b_id_j} + \mu_d \sum_{i,j} j \cdot dn_{b_id_j} \\ &= \mu_b dn_B + \mu_d dn_D. \end{aligned}$$

On the basis of the components alone, however, $dG^{liq} = \mu_B dn_B + \mu_D dn_D$ thus, the chemical potential of each component is equal to that of its unassociated species. Since

$$\mu_B = \mu_B^0 + RT \ln \gamma_B X_B = \mu_b = \mu_b^0 + RT \ln \gamma_b X_b \quad (2)$$

and $X_B = 1$ for the pure component B, the relationship between the standard states of component B and species b is

$$\mu_B^0 = \mu_b^0 + RT \ln \gamma_b^* X_b^* \quad (3)$$

where γ_b^* and X_b^* refer to the activity coefficient and mole fraction of species b in pure B. Substituting this expression for μ_B^0 in Equation 2 and eliminating the standard state chemical potential yields

$$\gamma_B = \frac{\gamma_b X_b}{X_B X_b^* \gamma_b^*} \quad \text{and} \quad \gamma_D = \frac{\gamma_d X_d}{X_D X_d^* \gamma_d^*}.$$

Therefore, the activities of the melt components are related to the activities of the unassociated melt species by

$$a_B = \frac{a_b}{X_b^* \gamma_b^*} \quad \text{and} \quad a_D = \frac{a_d}{X_d^* \gamma_d^*}.$$

For ideal associated mixtures $\gamma_b = \gamma_b^* = \gamma_d = \gamma_d^* = 1$, so that $\gamma_B = X_b / X_B X_b^*$ and

$$a_B = X_b / X_b^*. \quad (4)$$

Equation 4 indicates that even if disproportionation takes place in the melt at the P-T conditions of the melting curve of pure B [that is, a_b^m (= $X_b^m = X_b^{m*}$) is less than unity], a_B^m remains equal to unity. Here, m refers explicitly to the melt phase. As a result of not rigorously distinguishing between melt component and melt species, Burnham (1981) and Burnham and Nekvasil (1986) incorrectly assumed that $a_B^m = X_B^m$ and therefore that a_B^m would be less than unity along the melting curve of pure B.

For the simple association reaction b + d = bd the equilibrium constant can be formulated as

$$K_r = \frac{a_{bd}^m}{a_b^m a_d^m} = \frac{(X_B^m - X_b^m)}{X_b^m [X_D^m - (X_B^m - X_b^m)]} = \exp\left(-\frac{\Delta \overline{G}_r^0}{RT}\right)$$

where ΔG_r^0 contains the standard state chemical potentials of all melt species involved in the reaction. In this case of simple association, ideal mixing of the species leads to negative deviations from ideality of the components (e.g., $\gamma_B^m < 1$ and $\gamma_D^m < 1$, even though $\gamma_b^m = \gamma_d^m = \gamma_{bd}^m = 1$). In contrast, a speciation reaction involving formation of species b, bb, and d and ideal mixing of these species yield positive deviations from ideality for both components. As concluded by Hildebrand and Scott (1964, p. 179), if a more complex species (e.g., bbd) were produced, one component might show negative deviations from ideality for all concentrations, whereas the other component would show positive deviations over a certain portion of the compositional range and negative deviations over the remaining portion. For example, in the case of the production of species bbd and ideal mixing of the species, $\gamma_D > 1$ for $X_D > 0.5$ and $\gamma_D < 1$ for $X_D < 0.5$, whereas $\gamma_B < 1$ for all X_B although $\overline{G}^{ex} > 0$; see Appendix 1. Dolazalek (1908) suggested that even strong positive deviations from ideality of components can be modeled by ideal mixing of appropriate species. However, Hildebrand and Scott (1964, p. 188) have shown quite convincingly that for some systems the amount of association required may be unreasonable on a structural basis. Without non-thermodynamic data in support of the existence of the species, successful prediction of the phase equilibria does not constitute proof of the existence of the proposed species (e.g., Jordan, 1970). Justification of the use of the method lies in its ability to model, simply and successfully, the systems of interest and to predict reliably phase equilibria not used in the modeling. It can be stated, however, that the proposed species are visualized not as discrete individual units but rather as stoichiometric descriptions of a network in the melt.

Standard state Gibbs free energies

Modeling the mixing behavior in melts in the system Ab-Qz-H_2O requires formulation of appropriate standard states for the unassociated melt species, as well as for the components of the solid phases. There is now a significant data base of thermochemical and volumetric data on crystalline and liquid albite and quartz. Perhaps the best choice of a standard state results from the combination of data that are most consistent with the anhydrous melting curves of high albite and β quartz.

Albite. Figure 1 shows the envelope of anhydrous (Fig. 1a) and H_2O-saturated (Fig. 1b) melting curves for albite, calculated using a variety of thermochemical data for Ab liquid and high albite and the expression

$$\mu_{Ab}^{0m} - \mu_{Ab}^{0s} = -RT \ln \frac{X_{Ab}^m}{X_{Ab}^s} = 0 \qquad (6)$$

(and its modification for hydrous melts as provided by the albite-H_2O model of Burnham, 1975), where the available thermochemical data are assumed to describe the standard-state chemical potentials of Ab component in the liquid, m, and solid, s. Plotted for comparison are experimental phase equilibrium data in these systems. Standard-state enthalpy of formation, standard entropy, standard heat capacity, molar volume, expansivity, and compressibility data for crystalline high albite from Ghiorso et al. (1983), Holland and Powell (1990), Berman (1988, 1992), Robie et al. (1978), and Prewitt et al. (1976) and for liquid albite from Stebbins et al. (1983), Lange and Carmichael (1987), and Kress et al. (1988) were used in the construction of the envelopes in Figure 1.

Burnham (1981), Burnham and Nekvasil (1986), Navrotsky et al. (1982), and Kress et al. (1988) showed that the thermochemical and volumetric data that they used to formulate the standard states of crystalline and liquid albite yielded calculated melting curves in significant disagreement with experimental solidus data. Figure 1 shows that this disagreement is maintained regardless of the data selected for the standard state and is well outside analytical and experimental uncertainties. If this disagreement could be attributed specifically to the measured compressibility of albite melt, then it might arise from problems in ultrasonic measurements on high viscosity liquids, a result of the preparation method of the starting materials or inherent in the compositions investigated (since Kress et al., 1988, did not actually conduct measurement on melts of albite composition). Alternatively, the disagreement might indicate that the melts used in the compressibility measurements did not reflect the equilibrium structure of the liquid at elevated pressure, since they were conducted at 1 atm.

The disagreement between any specific calculated melting curve for albite and the solidus data can be removed by the use of complex pressure-dependent volume and compressibility expressions for the liquid (e.g., Navrotsky et al., 1982; Kress et al., 1988) obtained by regression of the Ab-H_2O melting curves that account for the pressure dependence of the standard enthalpies and entropies at P and T [because $(\partial H/\partial P)_T = V(1 - \alpha T)$ and $(\partial S/\partial P)_T = -\alpha V$]. The apparent need for a complex expression for the volume of fusion (Navrotsky et al., 1982) or for the compressibility of albite melt (Kress et al., 1988) could be interpreted as an indication of a strongly pressure-dependent disproportionation reaction in albite melts. The measured compressibility should provide information on the volume change of such disproportionation. However, the available compressibility data (Kress et al., 1988) do not permit agreement with albite and albite-H_2O solidus data and cannot be used for this purpose.

If the amount of disproportionation in albite melt is minor at 1 atm (and therefore the melt consists mainly of ab^m species at this pressure), then thermochemical and volumetric data obtained at 1 atm may be used to describe the thermal systematics of Ab melt component, as well as ab melt species at this pressure. However, if disproportionation increases with pressure, the thermochemical and volumetric data obtained at 1 atm would not include the heat of the disproportionation at elevated pressures and would not describe the standard state Gibbs free energy of albite melt component (μ_{Ab}^{0m}) at such pres-

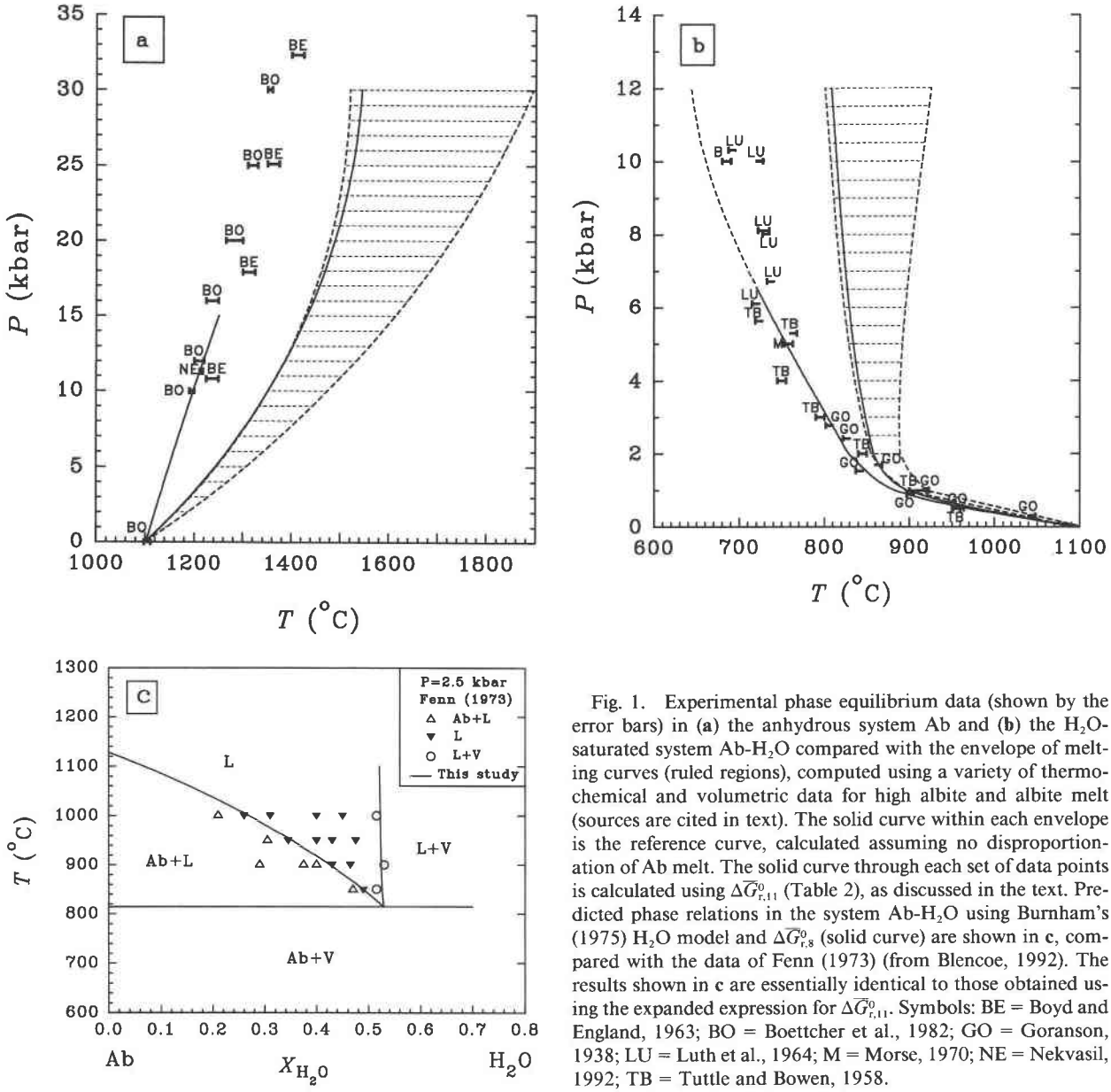

Fig. 1. Experimental phase equilibrium data (shown by the error bars) in (**a**) the anhydrous system Ab and (**b**) the H_2O-saturated system Ab-H_2O compared with the envelope of melting curves (ruled regions), computed using a variety of thermochemical and volumetric data for high albite and albite melt (sources are cited in text). The solid curve within each envelope is the reference curve, calculated assuming no disproportionation of Ab melt. The solid curve through each set of data points is calculated using $\Delta\overline{G}^{0}_{r,11}$ (Table 2), as discussed in the text. Predicted phase relations in the system Ab-H_2O using Burnham's (1975) H_2O model and $\Delta\overline{G}^{0}_{r,8}$ (solid curve) are shown in **c**, compared with the data of Fenn (1973) (from Blencoe, 1992). The results shown in **c** are essentially identical to those obtained using the expanded expression for $\Delta\overline{G}^{0}_{r,11}$. Symbols: BE = Boyd and England, 1963; BO = Boettcher et al., 1982; GO = Goranson, 1938; LU = Luth et al., 1964; M = Morse, 1970; NE = Nekvasil, 1992; TB = Tuttle and Bowen, 1958.

sures. The greater the amount of disproportionation in the melt and the greater the pressure dependence of this disproportionation, the more important the compressibility term becomes in describing the volume of albite melt component at elevated pressures and the less likely it will be that the 1-atm data (used with Eq. 6) could yield the real melting curve. If the difference between the calculated and real melting curves is due to disproportionation alone and not to significant changes in ab melt species with pressure, then the 1-atm data can be used to describe the standard-state chemical potential of the undissociated ab melt species. This assumption has been made here; the expression for the standard-state Gibbs free energy for albite melt species (μ^{0m}_{ab}) used in this study is given in Table 1. The relation between this standard-state Gibbs free energy and that for the albite component (Ab) is given by Equation 3.

The standard-state chemical potentials for ab melt species and Ab crystalline component can be used to construct a reference curve (Fig. 1) along which the a^{m}_{ab} remains equal to unity; that is, no disproportionation in the melt is considered. As this reference curve is a matter of choice within the envelope given by available thermochemical and volumetric data, the energy of any disproportionation at 1 atm may have been included in the standard state Gibbs free energy that we chose. In this case, calculated abundances of all species would represent minimum abundances.

When melt disproportionation is considered, calculation of the actual melting curve of albite requires use of

TABLE 1. Standard-state Gibbs free energy expressions for solid and liquid Ab and Qz (Si_4O_8)

Parameter	High Ab[A]	Liquid Ab	β-Qz[A]	Liquid Qz
$\overline{H}^0_r(P_r,T_r)$	−937 289	−942 430[B]	−868 668	−881 582[C]
$\overline{S}^0(P_r,T_r)$	53.64	30.88[D]	42.26	10.77[C]
$\overline{C}_P$ a	94.08	88.2[E]	76.49	83.16[F]
b	−577.32	0	−229.71	0
c	−1 886 431	0	−3 390 711	0
d	255 888 151	0	469 950 653	0
$\overline{V}^0(P_r,T_r)$	2.41	2.80[G]	2.27	2.85[H]
l	1	0	1	1
$a(\times10^{-5})$	2.6307	1.65[H]	0	−12.7620[I]
$b(\times10^{-9})$	3.2407	0[H]	0	51.8770[I]
$c(\times10^{-6})$	−1.9447	5.78[H]	−1.2383	−4.2826[I]
$d(\times10^{-11})$	0.48611	−26[H]	0.70871	−7.2571[I]
T_e	0	1373[H]	0	0

Note: $\overline{G}^0(P,T) = \overline{H}^0_r(P_r,T_r) + \int_{T_r}^{T} \overline{C}_P\,dT - T[\overline{S}^0(P_r,T_r) + \int_{T_r}^{T} \overline{C}_P/T\,dT] + \int_{P_r}^{P} \overline{V}(P,T)\,dP.$

$\overline{C}_P = a + b/T^{0.5} + c/T^2 + d/T^3.$

$l=0$: $\begin{cases} \overline{V}(P,T)/\overline{V}^0(P_r,T_r) = \exp[a(T-T_r) + 0.5b(T^2-T_r^2)]\exp\{-[c + d(T-T_e)](P-P_r)\}. \\ \alpha = a + bT,\ \beta = c + d(T-T_e). \end{cases}$

$l=1$: $\overline{V}(P,T)/\overline{V}^0(P_r,T_r) = 1 + a(T-T_r) + b(T-T_r)^2 + c(P-P_r) + d(P-P_r)^2.$

$P_r = 1$ bar, $T_r = 298.15$ K. Units are cal, K, and bars.

[A] Berman (1992).
[B] $\overline{H}^{0,l}_{Ab}(P_r,T_r) = \Delta\overline{H}^0_{fusion} + \overline{H}^{0,s}_{hAb} + \int_{T_r}^{Tm}(\overline{C}^s_{PhAb} - \overline{C}^l_{PAb})\,dT$. $T_m = 1373$ K (Boettcher et al., 1982); $\Delta\overline{H}_{fusion}(P_r,T)$ (Stebbins et al., 1983).
[C] Constrained by melting T of cristobalite at 1 bar.
[D] $\overline{S}^{0,l}_{Ab}(P_r,T_r) = \Delta\overline{H}^0_{fusion}/T_m + \overline{S}^{0,s}_{hAb} + \int_{T_r}^{Tm}(\overline{C}^s_{PhAb} - \overline{C}^l_{PAb})/T\,dT$.
[E] Stebbins et al. (1983).
[F] Ghiorso et al. (1983).
[G] Reduced from Kress et al. (1988) by −0.077.
[H] Lange and Carmichael (1987).
[I] Regression of Qz(-H_2O) solidi.

$$\mu^{0m}_{ab} - \mu^{0s}_{Ab} = -RT\ln\frac{X^m_{ab}}{a^s_{Ab}} > 0. \qquad (7)$$

Depending upon the amount of the dissociation (and therefore the deviation of X^m_{ab} from unity) the calculated melting temperatures could be significantly lower than the reference curve calculated by Equation 6. However, prediction of the real melting curve would require some independent means (e.g., quantitative spectroscopic investigation) of evaluating the equilibrium constant for the disproportionation reaction that would in turn yield the abundances of all species (including X^m_{ab}) at every P and T. As such independent data are not currently available, experimental solidus data are used here to calibrate $\Delta\overline{G}^0_r(P,T)$ (the change in standard-state Gibbs free energy of reaction) through the equilibrium constants of various proposed melt disproportionation reactions. The pressure dependence of $\Delta\overline{G}^0_r(P,T)$ thus includes the compressibility of albite melt component (that is, of dissociated albite melts).

Quartz. Figure 2 shows the envelopes of calculated melting curves for β quartz using standard-state enthalpy of formation, standard entropy, standard heat capacity, molar volume, expansivity, and compressibility data from Ghiorso et al. (1983), Holland and Powell (1990), Berman (1988, 1992), Robie et al. (1978), Richet et al. (1982), and Prewitt et al. (1976) for β quartz, and from Ghiorso et al. (1983), Stebbins et al. (1983), Kress et al. (1988), and Lange and Carmichael (1987) for molten silica. Unlike the case for albite, solidus data for β quartz lie inside the calculated envelope, indicating that agreement between the calculated melting curve of β quartz and the solidus data can be made through an appropriate choice of the available standard-state thermochemical data. Therefore, a^m_{Qz} can be considered equal to a^m_{qz}, and no disproportionation in pure silica melts needs to be considered. Thus the available standard-state thermochemical and volumetric data can be used to describe both Qz melt component and qz melt species (because $X^{m*}_{qz} = 1$).

The standard-state free energy expressions used in this study for Qz melt component (and hence qz melt species) are shown in Table 1 along with the sources of data. The compressibility and thermal expansivity are poorly known; therefore, values for these parameters were obtained by regressing solidus data to ensure consistency of the standard-state free energy with these data.

The system Ab-H_2O

Two modeling reactions were used in the system Ab-H_2O. The first reaction was formulated because of the incongruent melting of albite to jadeite and a silica-enriched liquid at ~33 kbar (Bell and Roseboom, 1969). At the singular point the chemical potential of jadeite in the liquid is equal to that of crystalline jadeite, and it is reasonable to conclude that there is some finite X^m_{jd} in the melt to account for this equality. Furthermore, it is also reasonable to consider that X^m_{jd} does not change from zero at some infinitesimally small pressure change below the singular point of the finite value at the singular point but instead may increase gradually with increasing pressure, until the chemical potentials are equal and crystalline jadeite is stabilized. For this reason a disproportionation reaction of albite species producing a jadeite and a silica

species was used in an attempt to model the deviation from the reference melting curve and the solidus data. In order to minimize the possibility that excess configuration entropy arising from mixing of very unlike molecules (e.g., those with major differences in molecular weight) plays a major role in inducing significant nonideal behavior (as in athermal solutions, Prigogene and Defay, 1954, p. 401), all melt species are expressed on an equal O basis [chosen here as 8, as done by Burnham (1981) and Hervig and Navrotsky (1984)].

If the deviation between the reference and the real melting curve for albite is a result of the disproportionation of ab melt species according to the following reaction:

$$\underset{\text{ab}}{NaAlSi_3O_8} \leftrightarrow 0.75\underset{\text{jd}}{Na_{1.33}Al_{1.33}Si_{2.67}O_8} + 0.25\underset{\text{qz}}{Si_4O_8} \quad (8)$$

then the equilibrium constant for this homogeneous melt reaction is given by

$$\Delta\overline{G}^0_{r,8}(P,T) = -RT \ln K_8$$

$$\text{where } K_8 = \frac{(X^m_{jd})^{0.75}(X^m_{qz})^{0.25}}{(X^m_{ab})} \quad (9)$$

if the melt is an ideal solution of species.

The amounts of jd^m and qz^m can be expressed by the deviation of X^m_{ab} (the mole fraction of the species ab) from X^m_{Ab} (the component mole fraction, which in the case of pure albite is equal to unity) through mass balance constraints to yield the following expressions: $X^m_{jd} = 0.75 \cdot (X^m_{Ab} - X^m_{ab})$ and $X^m_{qz} = 0.25 \cdot (X^m_{Ab} - X^m_{ab})$. Therefore,

$$K_8 = \frac{[0.75(X^m_{Ab} - X^m_{ab})]^{0.75}[0.25(X^m_{Ab} - X^m_{ab})]^{0.25}}{(X^m_{ab})}$$

$$= \frac{[0.75(1 - X^m_{ab})]^{0.75}[0.25(1 - X^m_{ab})]^{0.25}}{(X^m_{ab})}. \quad (10)$$

At each P and T along the albite solidus curve, X^m_{ab} can be obtained from the standard-state chemical potential expressions for ab^m melt species and crystalline albite (from Table 1) and from Equation 7. The values obtained can then be inserted into Equations 9 and 10 to solve for $\Delta\overline{G}^0_{r,8}(P,T)$.

In order to relate the activity of ab^m in hydrous albite melt to that in the anydrous melt at the same P and T, activity-composition relations between albite melt and H_2O must be known. In keeping with the concept of a speciation model the thermodynamic mixing properties of H_2O in albite melts should be based on a speciation reaction whose equilibrium constant is consistent with the spectroscopic data of Stolper (1982) and Silver and Stolper (1989), as well as on the *PVT* data of Burnham and Davis (1971) and all available H_2O-saturated and anhydrous phase equilibrium data. Although efforts are being made in this direction (Zeng and Nekvasil, unpublished manuscript), there is currently no model that is consistent with all these data. Alternatively, models based on *PVT* data (Burnham, 1975) or on application of Margules formalism to the regression of phase equilibrium

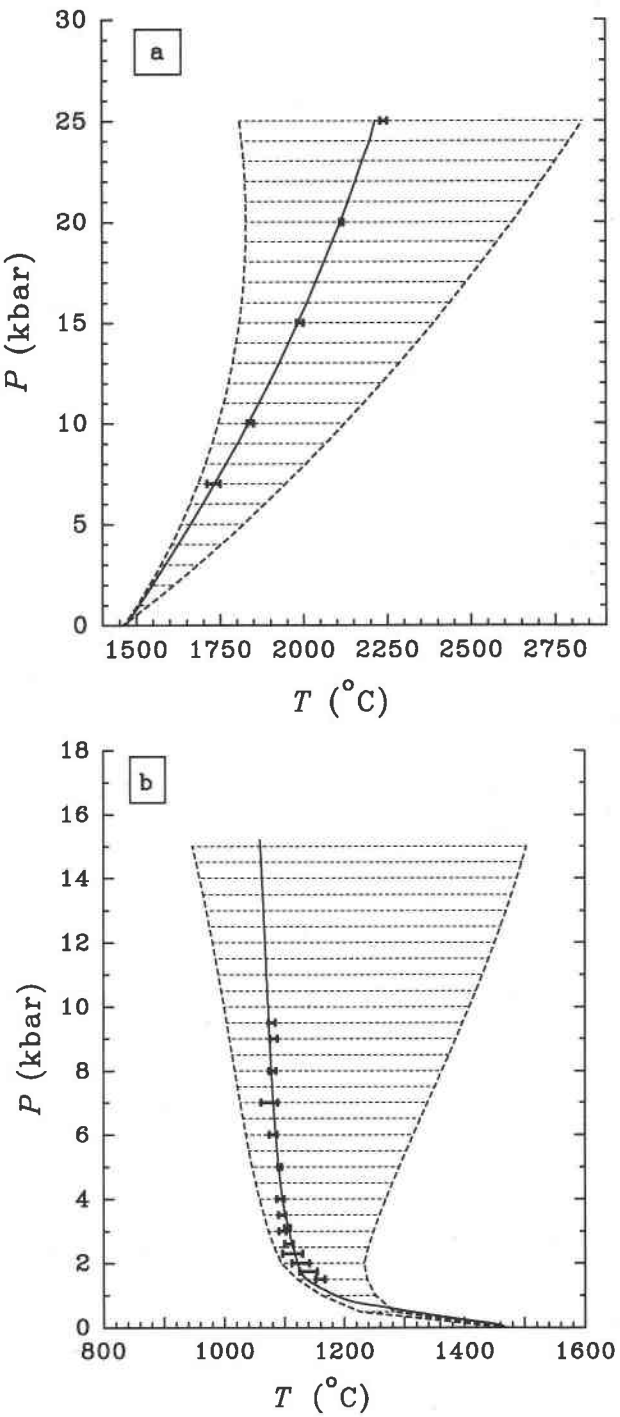

Fig. 2. Experimental phase equilibrium data (shown by the error bars) in (**a**) the anhydrous system Qz, and (**b**) the H_2O-saturated system Qz-H_2O, compared with the envelope of melting curves (ruled regions) computed using a variety of thermochemical and volumetric data for β quartz and Si_4O_8 melt (sources are in text). The solid curve within each envelope is the reference curve calculated assuming no disproportionation of Qz melt. Data are from Jackson (1976) in **a** and Kennedy et al. (1962) in **b**.

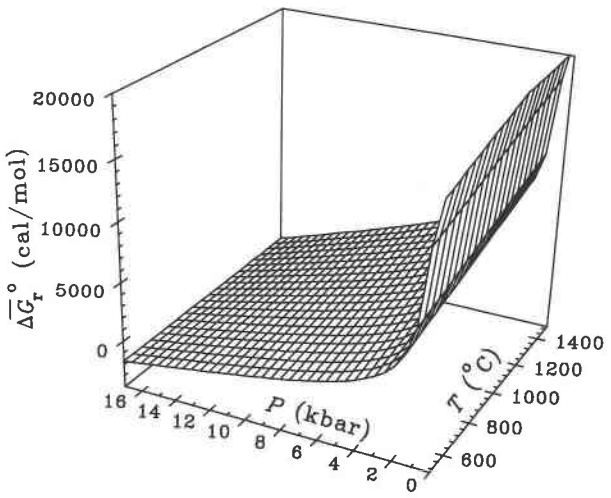

Fig. 3. Surface showing the variation in the change in standard-state Gibbs free energy of reaction for Reaction 8 as a function of pressure and temperature using the expression from Table 2, based only on the P-T solidus data in the system Ab-H_2O. The grid shows both isothermal sections and isobaric sections.

data (Blencoe, 1992) can be used. The model of Burnham (1975) is consistent with phase relations up to ~7 kbar, whereas that of Blencoe (1992) can be used only at 2.5 kbar. Neither model permits calculation of a possible second critical end point in this system (Paillat et al., 1992), but both appear to be reliable in the compositional region up to H_2O saturation. As the model of Burnham (1975) remains the most versatile for our purposes, it is used here. Importantly, since the quantification of Burnham's (1975) thermodynamic H_2O model did not use his proposed H_2O speciation model, use of his thermodynamic model here in no way indicates that we believe that H_2O completely dissociates to 2OH during dissolution in albite melt. We assume that the model of Burnham (1975) quantitatively describes the energetic effects of H_2O speciation reactions and that any remaining melt speciation reactions in hydrous albite melts can be described by the same reaction and equilibrium constant used to model anhydrous albite melt. This follows the principle of extension of the associated solution approach to higher order systems by adding equilibrium constants describing all relevant binary interactions. It assumes, of course, that there are no additional reactions between the species produced by pressure-induced dissociation and H_2O-induced dissociation of albite melt. Such an assumption is commonly used in the application of associated solution theory to ternary and higher order slag systems by using equilibrium constants calibrated in the bounding unary and binary systems (Barry et al., 1993). Justification of this assumption lies in the ability to predict phase relations. The fact that crystalline jadeite also appears as an incongruent melting product (at ~16 kbar; Boettcher and Wyllie, 1969) in the H_2O-saturated albite system implies that the use of Reaction 8 for anhydrous and hydrous albite melts is not unreasonable.

Figure 3 shows the surface representing $\Delta\overline{G}^0_{r,8}$ obtained by regressing the $\Delta\overline{G}^0_{r,8}$ data as a function of P and T and using the resulting expression (Table 2) to compute the characteristics of the surface. With an expression for $\Delta\overline{G}^0_{r,8}$, a^m_{ab} ($=X^m_{ab}$) can be calculated using Equations 9 and 10 for melts in the system albite-H_2O regardless of whether the melt is in equilibrium with crystalline albite. This in turn can yield μ^m_{ab} and μ^m_{Ab} at any P and T from Equation 2. Alternatively, $\Delta\overline{G}^0_{r,8}$ can be used to calculate melting curves in the system Ab-H_2O by solving for the two unknowns, T and X^m_{ab} (at a given P), using the two equations

$$\exp\frac{\Delta\overline{G}^0_{r,8}(P,T)}{RT} = \frac{[0.75(1 - X^m_{ab})]^{0.75}[0.25(1 - X^m_{ab})]^{0.25}}{(X^m_{ab})}$$

and

$$\mu^{0m}_{ab} - \mu^{0s}_{Ab} = -RT\ln\frac{X^m_{ab}}{a^s_{Ab}}.$$

Figure 1a and 1b show the anhydrous and H_2O-saturated melting curves of albite calculated using these expressions. As can be seen in Figure 1c, use of Burnham's (1975) H_2O model with our expression for $\Delta\overline{G}^0_{r,8}$ (calibrated along the H_2O-saturated and anhydrous albite solidi) results in excellent prediction of the phase relations in the system Ab-H_2O at 2.5 kbar throughout the H_2O-undersaturated region.

Kushiro (1980) found a significant change in properties such as density and viscosity of quenched albite melts near 15 kbar. That may imply that there are two types of speciation reactions in albite melts and that the modeling reaction involving the production of jd^m may not be useful at low pressures. Although two equilibrium constants must be simultaneously calibrated, for simplicity we investigate the effects of an alternate modeling reaction in the pressure region 1–10 kbar by assuming that one reaction dominates in the low-pressure region. The proximity of the stability field of a sodium silicate with stoichiometry $Na_2O{\cdot}2SiO_2$ in the system SiO_2-Na_2O-Al_2O_3 (Schairer and Bowen, 1956) is used to postulate an alternative modeling reaction in which a melt species ns^m and an aluminosilicate species als^m ($\frac{1}{2}Al_2O_3{\cdot}2SiO_2$, cf. dehydroxylated pyrophyllite, Burnham, 1981) in the following melt speciation reaction:

$$\underset{ab}{NaAlSi_3O_8} \leftrightarrow \underset{als}{0.6875Al_{1.45}Si_{2.91}O_8} + \underset{ns}{0.3125Na_{3.2}Si_{3.2}O_8}. \quad (11)$$

The $\Delta\overline{G}^0_{r,11}(P,T)$ for this reaction can be calibrated along the anhydrous and H_2O-saturated melting curves in the system Ab-H_2O using (1) the expression

$$\exp\left(-\frac{\Delta\overline{G}^0_{r,11}}{RT}\right) = \frac{[0.3125(X^m_{Ab} - X^m_{ab})]^{0.3125}[0.6875(X^m_{Ab} - X^m_{ab})]^{0.6875}}{(X^m_{ab})} \quad (12)$$

TABLE 2. Expression of standard-state Gibbs free energy of reaction

$$\Delta\overline{G}^0_r = a + bP + c/P^2 + (d + eP)T$$

Reaction no.	a ($\times 10^3$)	b ($\times 10^6$)	c ($\times 10^6$)	d	e ($\times 10^{-4}$)
8	−2.5414	6.3900	−6.7376	4.8987	−2.5353
11	−2.3853	6.3025	−6.2864	4.5446	−2.4565

$$\Delta\overline{G}^0_r = a + b\ln(P) + c/\ln(P + 1) + [d + e\ln(P) + f/P^2]T + [g + h\ln(P)]T^2$$

Reaction no.	a ($\times 10^5$)	b ($\times 10^4$)	c ($\times 10^5$)	d ($\times 10^2$)	e ($\times 10$)	f ($\times 10$)	g ($\times 10^{-1}$)	h ($\times 10^{-2}$)
11	−1.8174	1.8719	−1.2697	3.7854	−3.6962	9.9952	−1.4645	1.4293

Note: units are cal, K, and bars.

(2) the fact that X^m_{Ab} is equal to unity along the anhydrous melting curve of Ab (as is the anhydrous mole fraction of Ab along the H_2O-saturated solidus), and (3) X^m_{ab} from Equation 7. The expression obtained by regression of the resulting values of $\Delta\overline{G}^0_{r,11}(P,T)$ yields essentially the same melting curves as that obtained by using $\Delta\overline{G}^0_{r,8}(P,T)$. On the basis of the system Ab-H_2O alone, there is no independent means of deciding which reaction (Reaction 8 or 11) is preferable. It is shown below however, that each reaction results in significantly different predicted eutectic compositions in the system Ab-Qz-H_2O, and this difference provides a basis for selection of the better model reaction.

THE SYSTEM Ab-Qz-H_2O

The anhydrous solidus in the system albite-quartz-H_2O has been a source of experimental controversy. Figure 4 shows the available experimental solidus P-T data for both anhydrous and H_2O-saturated conditions. The anhydrous solidus temperatures of Luth (1969) are consistent with the new reversed data of Nekvasil (1992), and both sets of data lie at significantly higher temperatures than do the data of Boettcher et al. (1984). Therefore, the data of Boettcher et al. (1984) were not used for this portion of the study.

Luth et al. (1964) and Tuttle and Bowen (1958) investigated the phase relations of albite under H_2O-saturated conditions. Although these investigations were conducted at different pressures, extrapolation of the lower pressure data of Tuttle and Bowen yields a melting curve that lies at lower temperatures than indicated by the data of Luth et al. (1964); however, the differences are not great (Fig. 4b). Recent reversed higher pressure experiments of Nekvasil (1992) were consistent with the H_2O-saturated P-T data of Luth et al. (1964).

Several workers have attempted to locate the eutectics in the anhydrous and H_2O-saturated system Ab-Qz. Figure 5 shows the available compositional data. Note that even for the widely differing eutectic compositions obtained by the few workers in the dry system, all the data (as well as recent results of Johannes, 1993 personal communication) indicate that the effect of increasing H_2O content is the contraction of the quartz + liquid field, in contrast with the conclusions of Pichavant et al. (1992).

Modeling the thermodynamic mixing behavior of melts in the system Ab-Qz-H_2O using associated solution theory can be conducted in three ways: (1) assuming no dissociation or interaction between melt species, (2) assuming that the only speciation in this system is a result of disproportionation of albite species and that there is no interaction between quartz and albite species, or (3) assuming that two or more reactions take place, one involving dissociation of albite species, and the others describing interactions between albite and quartz species and perhaps between new species arising from component interactions.

Method 1

The Ab + Qz solidus temperatures can be calculated using the standard-state Gibbs free energy functions in Table 1, assuming that there is no dissociation or interaction (i.e., the $a^m_{ab} = a^m_{Ab} = X^m_{ab}$). As shown in Figure 4, the calculated temperatures are significantly higher than those of the solidus data. Eutectic compositions can be calculated using Equation 7 and substituting X^m_{Ab} for X^m_{ab} (Fig. 5). The lack of agreement between the calculated and experimental eutectic compositions appears to indicate significant nonideal behavior of the melt components and that method 1 cannot be used to model mixing behavior in this system.

Method 2

If dissociation of ab^m but no interaction between ab^m and qz^m species is considered, then for the ns^m-producing Reaction 11 there will be four species in the system Ab-Qz: ab^m, qz^m, als^m, and ns^m, where als^m and ns^m are produced only by the dissociation of ab^m. For pure albite melt, $X_{Ab} = 1$ and

$$K^* = \frac{X^{m*}_{als}{}^{0.6875} \cdot X^{m*}_{ns}{}^{0.3125}}{X^{m*}_{ab}}$$

$$= \frac{[0.6875\cdot(1 - X^{m*}_{ab})]^{0.6875}\cdot[0.3125\cdot(1 - X^{m*}_{ab})]^{0.3125}}{X^{m*}_{ab}}$$

whereas within the system Ab-Qz, where $X^m_{Ab} \neq 1$,

$$K = \frac{X^{m}_{als}{}^{0.6875} \cdot X^{m}_{ns}{}^{0.3125}}{X^{m}_{ab}}$$

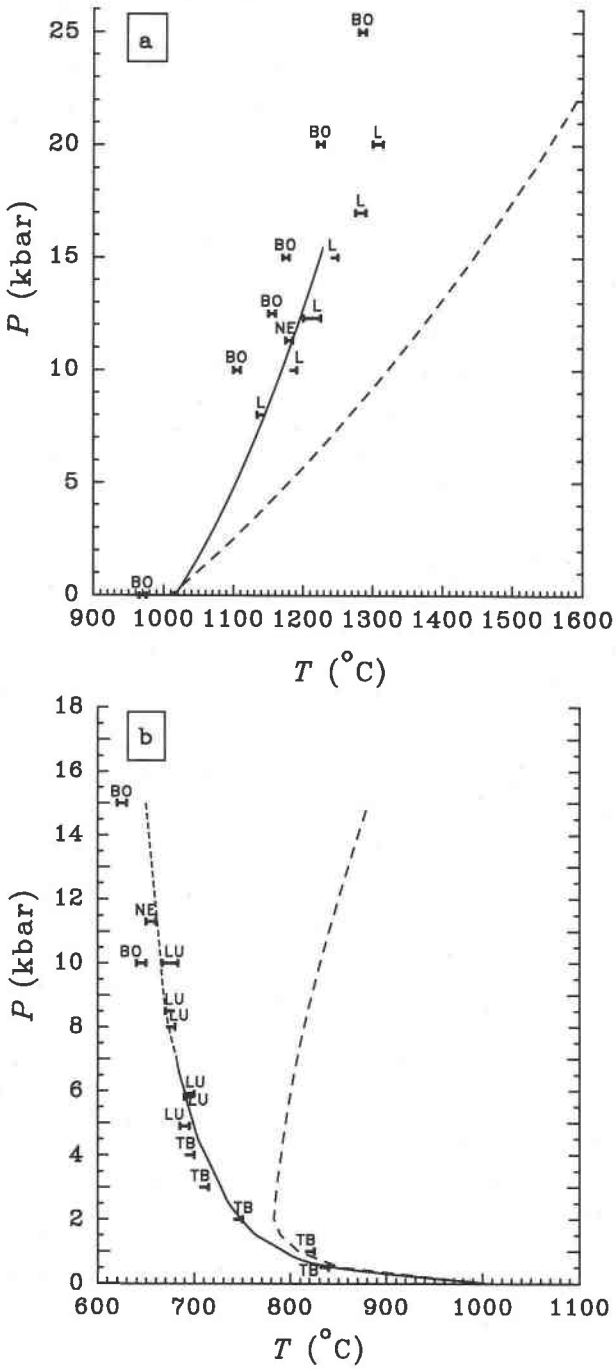

Fig. 4. Experimental phase equilibrium data (shown by the error bars) in (**a**) the anhydrous system Ab-Qz, and (**b**) the H_2O-saturated system Ab-Qz-H_2O, compared with the solidus curves (solid curves) calculated using the expanded expression for $\Delta G^0_{r,111}$, assuming that the ns^m-producing reaction is the only speciation reaction occurring in these systems (and that there is no interaction between ab^m and qz^m melt species). The dashed extension of the calculated solidus curves in **b** indicates the location of the calculated solidus at pressures above the recommended limit of applicability of the albite-H_2O solution model of Burnham (1975). The dashed curves indicate the reference curves calculated assuming no speciation at all and, therefore, that $\mu^0_{ab} = \mu^0_{Ab}$. Symbols: BO = Boettcher et al., 1984; LU = Luth et al., 1964; L = Luth, 1969; NE = Nekvasil, 1992; TB = Tuttle and Bowen, 1958.

←

From Equation 4 this implies that $a^m_{Ab} = X^m_{Ab}$. This result in combination with the relation $X^m_{Qz} = X^m_{qz} = a^m_{Qz}$ (because method 2 assumes no interaction of qz^m species with ab^m species and no disproportionation in pure silica melts) indicates that the melt components Ab and Qz must mix ideally, even though $a_{Ab} > a_{ab}$. That this result is specific to the reaction chosen and not a general result of using method 2 can be seen by using the jd^m-producing reaction (Reaction 8).

$$K^* = \frac{[0.75\cdot(1 - X^{m*}_{ab})]^{0.75}\cdot[0.25\cdot(1 - X^{m*}_{ab})]^{0.25}}{X^{m*}_{ab}}$$

and

$$K = \frac{[0.75\cdot(X^m_{Ab} - X^{m*}_{ab})]^{0.75}\cdot[0.25\cdot(X^m_{Ab} - X^m_{ab})]^{0.25}}{X^m_{ab}}.$$

Ideal mixing of the components requires that substitution of X^m_{ab}/X^*_{ab} for X^m_{Ab} according to Equation 4 permits K to equal K^*. This substitution leads to the following expression:

$$0.25\cdot(1 - X^{m*}_{ab}) = 0.25\cdot(1 - X^{m*}_{ab}) + \frac{X^m_{Qz}}{X^m_{Ab}}$$

which holds true only for $X^m_{Qz} = 0$; therefore, the jd^m-producing reaction (Reaction 8) does not result in ideal mixing of the components.

Because each unique stoichiometric relation has specific implications for the thermodynamic mixing behavior of the components, the best modeling reaction can be selected by evaluating predictive abilities within the Ab-Qz system. As was done with method 1, eutectic compositions were calculated using Equations 7 and 10 for both Ab and Qz. The dashed curves in Figure 5 show the predicted eutectic compositions for the jd^m-producing reaction (Reaction 8) and the solid curves those for the ns^m-producing reaction (Reaction 11). It is apparent that eutectic compositions predicted using Reaction 11 show remarkable agreement with the anhydrous and H_2O-saturated experimental data. In contrast, eutectic compositions cannot be predicted by Reaction 11. Because each reaction yields such different predicted eutectic compo-

$$= \frac{[0.6875\cdot(X^m_{Ab} - X^{m*}_{ab})]^{0.6875}\cdot[0.3125\cdot(X^m_{Ab} - X^m_{ab})]^{0.3125}}{X^m_{ab}}.$$

At P and T, $K = K^*$ and

$$\frac{[(1 - X^{m*}_{ab})]}{X^{m*}_{ab}} = \frac{[(X^m_{Ab} - X^{m*}_{ab})]}{X^m_{ab}}$$

which reduces to $\frac{X^m_{ab}}{X^{m*}_{ab}} = X^m_{Ab}$.

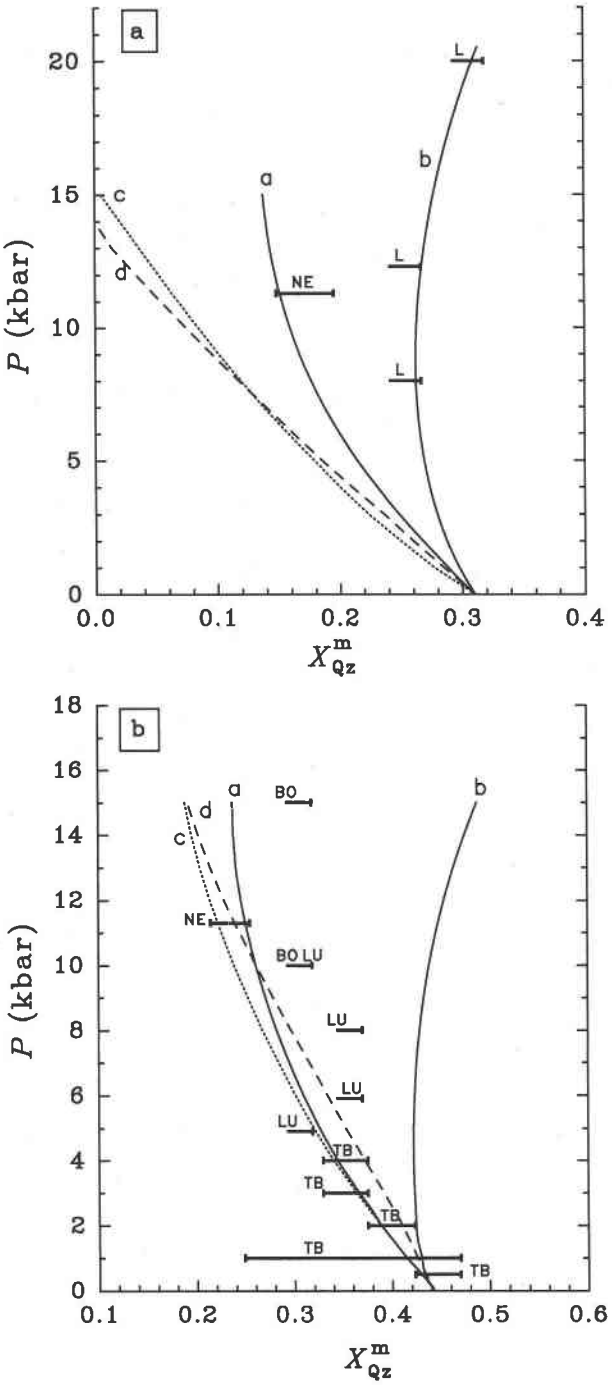

Fig. 5. Experimental eutectic compositional data (shown by the error bars) in (a) the anhydrous system Ab-Qz, and (b) the H_2O-saturated system Ab-Qz-H_2O, compared with curves calculated using the ns^m-producing reaction only (curve a), no speciation (curve b), the jd^m-producing reaction only (curve c), and speciation according to both Reactions 8 and 13 (curve d). Symbols: L = Luth, 1969; LU = Luth et al., 1964; NE = Nekvasil, 1992; TB = Tuttle and Bowen, 1958; BO = Boettcher et al., 1984.

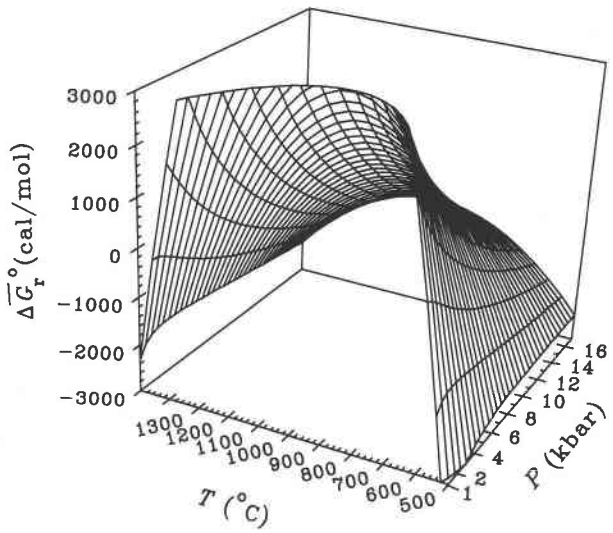

Fig. 6. Surface showing the variation in the change in standard-state molar Gibbs free energy of reaction for Reaction 11 as a function of pressure and temperature with the expanded expression from Table 2 calibrated from *P-T* data in the systems Ab-H_2O and Ab-Qz-H_2O. The grid gives both isothermal sections and isobaric sections.

sitions, it is evident that speciation reactions represent very sensitive modeling tools.

The expression for $\Delta G^0_{r,11}$ in Table 2 does not yield adequate calculated solidus temperatures in the system Ab-Qz-H_2O if only the temperatures along the dry and H_2O-saturated Ab solidi are used in its calibration. For this reason, the *P-T* data (not the compositional data) of the Ab + Qz solidus were used in conjunction with the *P-T* data of the albite solidus to provide lower temperature constraints on $\Delta G^0_{r,11}$. Regression of the combined data yields the expanded expression for $\Delta G^0_{r,11}$ in Table 2; the resulting free energy surface describing the expanded function is shown in Figure 6. The calculated solidus curves in Figure 1 indicate the quality of the fit. The predicted eutectic compositions are essentially unaffected by use of the expanded expression. Figure 7 shows the variations in calculated abundances of model species with pressure. The continuous nature of these variations differs from the results of Burnham and Nekvasil (1986).

Table 3 shows the predicted eutectic compositions and temperatures using the expanded expression for $\Delta G^0_{r,11}$ in Table 2 and method 2. The activities (or mole fractions in this case of ideal associated solutions) of the melt species ab^m and qz^m are also given. Importantly, at any pressure investigated, X^m_{qz} (on an anhydrous basis) is equal to the X^m_{Qz} of the eutectic composition, but X^m_{ab} deviates increasingly from X^m_{Ab} with increasing pressure (that is, the abundance of ab^m declines continuously with increasing pressure). The activity of the Ab melt component (a^m_{Ab}) at each *P-T* point of the calculated melting curves can be calculated by first obtaining X^{m*}_{ab} from Equation 10 (setting $X^m_{Ab} = 1$) and then substituting this value, as well as

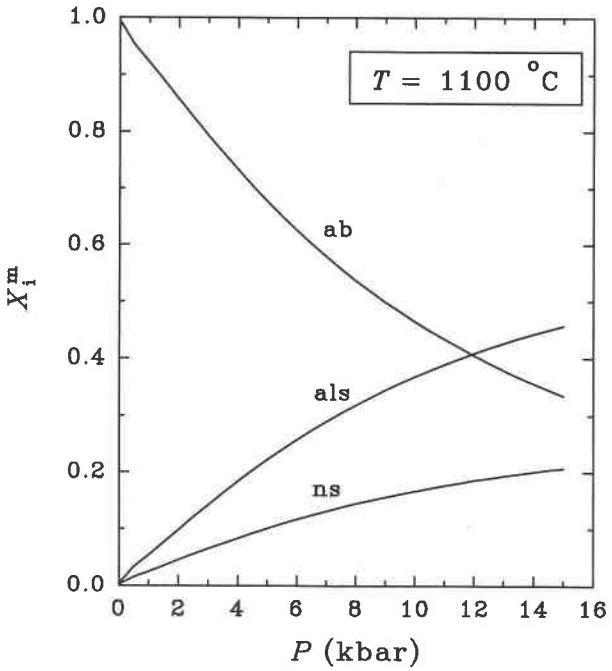

Fig. 7. Calculated variations in abundance (mole fractions of the melt) of species a as a function of pressure at 1100 °C for $X^m_{Ab} = 1$.

TABLE 3. Variation in the calculated eutectic temperatures, compositions, and activities of melt species and components with pressure

P (kbar)	T (°C)	X^m_{Qz}	a^m_{qz}	a^m_{ab}	a^m_{Qz}	a^m_{Ab}
			Anhydrous			
0.001	1009	0.310	0.310	0.683	0.310	0.690
1	1036	0.288	0.288	0.668	0.288	0.712
2	1058	0.268	0.268	0.640	0.268	0.732
3	1076	0.249	0.249	0.605	0.249	0.751
4	1092	0.231	0.231	0.567	0.231	0.769
5	1106	0.215	0.215	0.529	0.215	0.786
6	1119	0.200	0.200	0.492	0.200	0.800
7	1132	0.188	0.188	0.457	0.188	0.812
8	1144	0.177	0.177	0.425	0.177	0.823
9	1155	0.167	0.167	0.396	0.167	0.833
10	1167	0.159	0.159	0.369	0.159	0.841
11	1179	0.153	0.153	0.344	0.153	0.847
12	1191	0.147	0.147	0.322	0.147	0.853
13	1203	0.143	0.143	0.302	0.143	0.857
14	1215	0.140	0.140	0.284	0.140	0.860
15	1228	0.138	0.138	0.268	0.138	0.862
			H_2O-saturated			
0.001	1007	0.421	0.421	0.680	0.421	0.579
1	793	0.397	0.397	0.551	0.397	0.603
2	749	0.395	0.395	0.486	0.395	0.605
3	734	0.375	0.375	0.442	0.375	0.625
4	720	0.355	0.355	0.399	0.355	0.645
5	706	0.335	0.335	0.358	0.335	0.665
6	693	0.317	0.317	0.320	0.317	0.683
7	682	0.300	0.300	0.287	0.300	0.700

the calculated value for X^m_{ab} from Table 3, into Equation 4. The resulting ideal mixing behavior of components in this system is in accord with the calorimetric results of Hervig and Navrotsky (1984) and differs from the negative deviations from ideality calculated by Burnham (1981) and Burnham and Nekvasil (1986).

Figure 8a shows the calculated Ab + Qz solidus curves for different X^m_w from anhydrous to H_2O-saturated conditions based on method 2; calculated isobaric phase relations are shown in Figure 8b. Note that the shift of the eutectic compositions with increasing H_2O content is toward Qz, consistent with the data in Figure 5. Figure 8c shows the variation in the abundances of species along the Ab and Qz liquidi under anhydrous conditions at 5 kbar pressure. The inflection of each curve in Figure 8c reflects the differences in T-X slope between the Qz liquidus and the Ab liquidus and occurs at the eutectic (and therefore at the intersection of these liquidi).

Method 3

This approach involves consideration of multiple homogeneous melt equilibria. If, for example, the jd^m-producing Reaction (Reaction 8) is considered for albite melts, then an additional modifying reaction must take place upon the addition of Qz melt component. The combination of any set of stoichiometric relations has specific thermodynamic consequences. The following reactions,

$$\underset{ab}{NaAlSi_3O_8} \leftrightarrow 0.75\underset{jd}{Na_{1.33}Al_{1.33}Si_{2.67}O_8} + 0.25\underset{qz}{Si_4O_8} \quad (8)$$

and

$$\underset{ab}{NaAlSi_3O_8} + 0.0833\underset{qz}{Si_4O_8} \leftrightarrow 0.3958\underset{nds}{Na_{2.53}Si_{3.37}O_8} + 0.6875\underset{als}{Al_{1.46}Si_{2.91}O_8} \quad (13)$$

(where nds^m is a sodium silicate with a 3:4 ratio of Na:Si), describe disproportionation and interaction in the system Ab-Qz-H_2O. The following equilibrium constants can be formulated:

$$\Delta G^0_{r,8} = -RT \ln K_8$$
$$= -RT(0.7500 \ln X^m_{jd} + 0.2500 \ln X^m_{qz} - \ln X^m_{ab})$$

and

$$\Delta G^0_{r,13} = -RT \ln K_{13}$$
$$= -RT(0.3958 \ln X^m_{nds} + 0.6895 \ln X^m_{als} - \ln X^m_{ab} - 0.0833 \ln X^m_{qz}). \quad (14)$$

Values of X^m_{qz} and X^m_{ab} can be calculated along the eutectic melting curve using the expressions in Table 1 and combined with mass balance and cation balance expressions to obtain the mole fractions of jd^m, nds^m, and als^m species as functions of $X^m_{Ab} - X^m_{ab}$ and $X^m_{Qz} - X^m_{qz}$. The resulting expressions can be used with $\Delta G^0_{r,8}$ to obtain $\Delta G^0_{r,13}$ and X^m_{Ab}. Assessment of the set of Reactions 8 and 13 in modeling mixing behavior in this system was conducted by comparing available eutectic compositional data with those compositions predicted. The short-dashed curves in Figure 5 show that the predicted compositions are in poor agreement with the compositional data. They

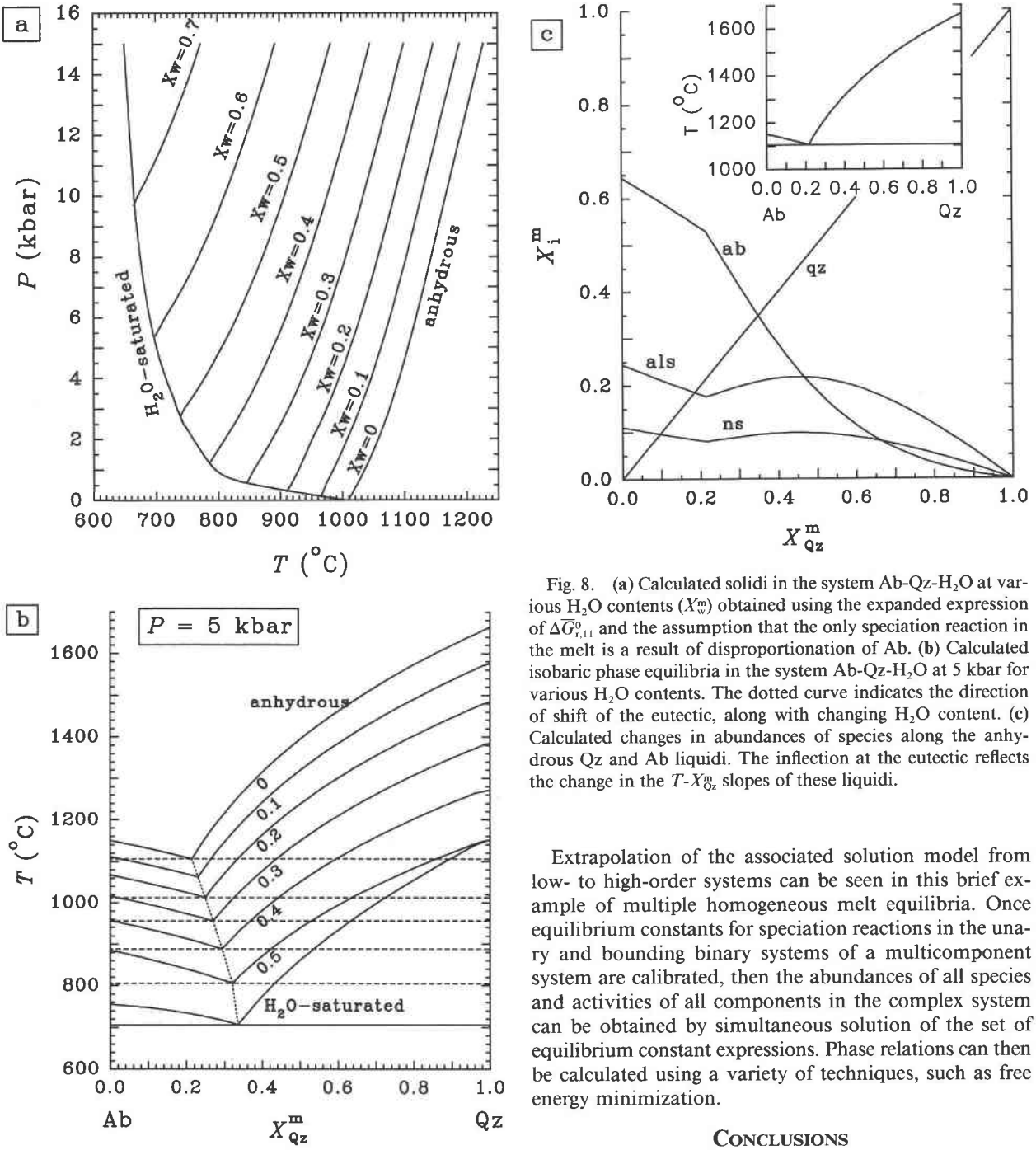

Fig. 8. (**a**) Calculated solidi in the system Ab-Qz-H_2O at various H_2O contents (X_w^m) obtained using the expanded expression of $\Delta\overline{G}^0_{r,11}$ and the assumption that the only speciation reaction in the melt is a result of disproportionation of Ab. (**b**) Calculated isobaric phase equilibria in the system Ab-Qz-H_2O at 5 kbar for various H_2O contents. The dotted curve indicates the direction of shift of the eutectic, along with changing H_2O content. (**c**) Calculated changes in abundances of species along the anhydrous Qz and Ab liquidi. The inflection at the eutectic reflects the change in the T-X^m_{Qz} slopes of these liquidi.

also show poor agreement with the few available anhydrous compositional data.

Reaction 13 is only one example of numerous possible reactions that can be proposed. However, when considering the jd^m-producing disproportionation reaction, it is difficult to postulate any interaction between ab^m and qz^m species that would sufficiently counteract the production of qz^m by dissociation (while preserving the large deviation of X^m_{ab} from X^m_{Ab}), enabling reliable prediction of phase relations in this system.

Extrapolation of the associated solution model from low- to high-order systems can be seen in this brief example of multiple homogeneous melt equilibria. Once equilibrium constants for speciation reactions in the unary and bounding binary systems of a multicomponent system are calibrated, then the abundances of all species and activities of all components in the complex system can be obtained by simultaneous solution of the set of equilibrium constant expressions. Phase relations can then be calculated using a variety of techniques, such as free energy minimization.

Conclusions

Phase relations in the system Ab-Qz-H_2O can be modeled using ideal associated solution theory. Only disproportionation in the system Ab-H_2O needs to be considered to predict reliably anhydrous and H_2O-saturated phase relations in this system; no nonideal terms are needed. As is evident from the above analysis, each stoichiometric relation used in modeling has distinct thermodynamic implications that are reflected in the predicted phase relations, thus making speciation reactions sensitive modeling tools. Although modeling of the mixing behavior in the system Ab-Qz-H_2O is undoubtedly

simple relative to many other systems of geologic relevance, associated solution theory (both ideal and regular) promises a ready means of modeling systems such as anorthite-forsterite, in which compound formation (in the form of spinel) is exhibited, as well as systems in which complex nonideal behavior such as liquid immiscibility occurs.

Acknowledgments

H.N. would like to thank C. Wayne Burnham for teaching her to look beyond the beaten path. The careful review of R. Nielsen led to many improvements of the manuscript. The support of the Center for High Pressure Research and of NSF grant EAR-91-17215 (to H.N.) is gratefully acknowledged. CHiPr manuscript no. 110.

References cited

Barry, T.I., Dinsdale, A.T., and Gisby, J.A. (1993) Predictive thermochemistry and phase equilibria of slags. Journal of the Minerals, Metals, and Materials Society, 45(4), 32–38.

Bell, P.M., and Roseboom, E.H., Jr. (1969) Melting relationships of jadeite and albite to 45 kilobars with comments on melting diagrams of binary systems at high pressures. Mineralogical Society Special Paper, 2, 151–162.

Berman, R.G. (1988) Internally-consistent thermodynamic data for minerals in the system MgO-FeO-Fe_2O_3-Al_2O_3-SiO_2-TiO_2-H_2O-CO_2. Journal of Petrology, 29, 445–522.

——— (1992) TWEEQU software (version 1.0): Thermobarometry with estimation of equilibration state. Geological Society of Canada, Ottawa, Canada.

Blencoe, J.G. (1992) A two-parameter Margules method for modelling the thermodynamic mixing properties of albite-water melts. Transactions of the Royal Society of Edinburgh, Earth Sciences, 83, 423–428.

Boettcher, A.L., and Wyllie, P.J. (1969) Phase relationships in the system $NaAlSiO_4$-SiO_2-H_2O to 35 kilobars pressure. Geochimica et Cosmochimica Acta, 32, 999–1012.

Boettcher, A.L., Burnham, C.W., Windom, K.E., and Bohlen, S.R. (1982) Liquids, glasses, and the melting of silicates to high pressures. Journal of Geology, 90, 127–138.

Boettcher, A.L., Guo, Q., Bohlen, S.R., and Hanson, B. (1984) Melting in feldspar-bearing systems to high pressures and the structures of aluminosilicate liquids. Geology, 12, 202–204.

Boyd, F.R., and England, J.L. (1963) Effect of pressure on the melting of diopside, $CaMgSi_2O_6$, and albite, $NaAlSi_3O_8$, in the range up to 50 kilobars. Journal of Geophysical Research, 68, 311–323.

Burnham, C. Wayne (1975) Water and magmas: A mixing model. Geochimica et Cosmochimica Acta, 39, 1077–1084.

——— (1981) Nature of multicomponent aluminosilicate melts: Chemistry and geochemistry of solutions at high temperatures and pressures, p. 127–229. Pergamon, Oxford England.

Burnham, C. Wayne, and Davis, N.F. (1971) The role of H_2O in silicate melts. I. *PVT* relations in the system $NaAlSi_3O_8$-H_2O to 10 kbar and 1000 °C. American Journal of Science, 270, 54–79.

Burnham, C. Wayne, and Nekvasil, H. (1986) Equilibrium properties of granite pegmatite magmas. American Mineralogist, 71, 239–263.

Chuang, Y.-Y., and Chang, Y.A. (1982) Extension of the associated solution model to ternary metal-sulphur melts: Cu-Ni-S. Metallurgical Transactions, 13B, 379–385.

Dolazalek, F. (1908) Zur Theorie der binaren Gemische und konzentrierten Lösungen. Zeitschift für physikalische Chemie, 64, 727–747.

Fenn, P.M. (1973) Nucleation and growth of alkali feldspars from melts in the system $NaAlSi_3O_8$-$KAlSi_3O_8$-H_2O. Ph.D. thesis, Stanford University, Stanford, California.

Ghiorso, M.S., Carmichael, I.S.E., Rivers, M.L., and Sack, R.O. (1983) The Gibbs free energy of mixing of natural silicate liquids, an expanded regular solution approximation for the calculation of magmatic intensive variables. Contributions to Mineralogy and Petrology, 84, 107–145.

Goranson, R.W. (1938) Silicate-water systems: Phase equilibria in the $NaAlSi_3O_8$-H_2O and $KAlSi_3O_8$-H_2O systems at high temperatures and pressures. American Journal of Science, 235A, 72–91.

Hervig, R.L., and Navrotsky, A. (1984) Thermochemical study of glasses in the system $NaAlSi_3O_8$-$KAlSi_3O_8$-Si_4O_8 and the join $Na_{1.6}Al_{1.6}Si_{2.4}O_8$-$K_{1.6}Al_{1.6}Si_{2.4}O_8$. Geochimica et Cosmochimica Acta, 48, 513–522.

Hildebrand, J.H., and Eastman, E.D. (1915) The vapor pressure of thallium amalgams. Journal of the American Chemical Society, 37, 2452.

Hildebrand, J.H., and Scott, R.L. (1964) The solubility of nonelectrolytes, 488 p. Dover, New York.

Holland, T.J.B., and Powell, R. (1990) An enlarged and updated internally consistent thermodynamic dataset with uncertainties and correlations in the system K_2O-Na_2O-CaO-MgO-FeO-Fe_2O_3-Al_2O_3-TiO_2-SiO_2-C-H_2-O_2. Journal of Metamorphic Geology, 8, 89–124.

Jackson, I. (1976) Melting of the silica isotypes SiO_2, FeF_2, and GeO_2 at elevated pressures. Physics of the Earth and Planetary Interiors, 13, 218–223.

Jordan, A.S. (1970) A theory of regular associated solutions applied to liquidus curves in the Zn-Te and Cd-Te systems. Metallurgical Transactions, 1, 239–249.

Kennedy, G.C., Wasserburg, G.J., Heard, H.C., and Newton, R.C. (1962) The upper three-phase region in the system SiO_2-H_2O. American Journal of Science, 260, 501–521.

Kress, V.C., Williams, Q., and Carmichael, I.S.E. (1988) Ultrasonic investigations of melts in the system Na_2O-Al_2O_3-SiO_2. Geochimica et Cosmochimica Acta, 52, 283–293.

Kushiro, I. (1980) Viscosity, density and structure of silicate melts at high pressures, and their petrological applications. In R.B. Hargraves, Ed., Physics of magmatic processes, p. 93–117. Princeton University Press, Princeton, New Jersey.

Lange, R., and Carmichael, I.S.E. (1987) Densities of Na_2O-K_2O-CaO-MgO-FeO-Fe_2O_3-Al_2O_3-TiO_2-SiO_2 liquids: New measurements and derived partial molar properties. Geochimica et Cosmochimica Acta, 51, 2931–2946.

Luth, W.C. (1969) The systems Ab-Qz and Sa-Qz to 20 kbar and the relationship between H_2O content, P_{H_2O} and P_T in granitic magmas. American Journal of Science, 267A, 325–341.

Luth, W.C., Jahns, R., and Tuttle, F. (1964) The granite system at pressures of 4 to 10 kbar. Journal of Geophysical Research, 69, 759–773.

Marcus, Y. (1977) Introduction to liquid state chemistry, 357 p. Wiley-Interscience, New York.

Morse, S.A. (1970) Alkali feldspars with water at 5 kbar pressure. Journal of Petrology, 11, Paer 2, 221–251.

Navrotsky, A., Capobianco, C., and Stebbins, J. (1982) Some thermodynamic and experimental constraints on the melting of albite at atmospheric and high pressure. Journal of Geology, 90, 679–698.

Nekvasil, H. (1992) Experimental constraints on anhydrous phase equilibria in the granite system. Proceedings of the IV International Symposium of Experimental Mineralogy, Petrology, and Geochemistry, Clermont-Ferrand, France, 26.

Paillat, O., Elphick, S.C., and Brown, W.L. (1992) The solubility of water in $NaAlSi_3O_8$ melts: A reexamination of Ab-H_2O phase relationships and critical behavior at high pressures. Contributions to Mineralogy and Petrology, 112, 490–500.

Pichavant, M., Holtz, F., and McMillan, P.F. (1992) Phase relations and compositional dependence of H_2O-solubility in quartz-feldspar melts. Chemical Geology, 96, 303–319.

Prewitt, C.T., Sueno, S., and Papike, J.J. (1976) The crystal structure of high albite and monalbite at high temperatures. American Mineralogist, 61, 1213–1225.

Prigogene, I., and Defay, R. (1954) Chemical thermodynamics: Treatise on thermodynamics based on the methods of Gibbs and De Donder, vol. 1, 543 p. Longmans, London, England.

Richet, P., Bottinga, Y., Denielou, L., Petitet, J.P., and Tequi, C. (1982) Thermodynamic properties of quartz, cristobalite, and amorphous silica: Drop calorimetry measurements between 1000 and 1800 K and a review from 0 to 2000 K. Geochimica et Cosmochimica Acta, 46, 2639–2658.

Robie, R.A., Hemingway, B.S., and Fisher, J.R. (1978) Thermodynamic properties of minerals and related mixtures at 298K and 1 bar (10^5

pascals) pressure and high temperatures. U.S. Geological Survey Bulletin, 1452, 456 p.
Schairer, J.F., and Bowen, N.L. (1956) The system Na_2O-Al_2O_3-SiO_2. American Journal of Science, 254, 129–195.
Shaw, H.R. (1968) Chemical states of H_2O and reaction in silicate-H_2O liquids and glasses. Geological Society of America Special Paper, 121, 274.
Silver, L., and Stolper, E.M. (1985) A thermodynamic model for hydrous silicate melts. Journal of Geology, 93, 161–178.
——— (1989) Water in albitic glasses. Journal of Petrology, 30, 667–709.
Stebbins, J.F., Carmichael, I.S.E., and Weill, D.E. (1983) The high temperature liquid and glass heat contents and the heats of fusion of diopside, albite, sanidine and nepheline. American Mineralogist, 68, 717–730.
Stolper, E.M. (1982) The speciation of water in silicate melts. Geochimica et Cosmochimica Acta, 46, 2609–2620.
Tuttle, O.F., and Bowen, N.L. (1958) Origin of granite in the light of experimental studies in the system $NaAlSi_3O_8$-$KAlSi_3O_8$-SiO_2-H_2O. Geological Society of American Memoirs, 74, 1–153.

Manuscript received May 19, 1993
Manuscript accepted November 8, 1993

Appendix 1. Modeling nonideal behavior of components in ideal associated solutions: Some examples

The following examples of interactions among species are discussed below to demonstrate specifically the use of speciation reactions and the assumption of ideal mixing of the species to model nonideal behavior of components: (1) simple association (i.e., b + d = bd), (2) complex association (i.e., 2b + d = b_2d), and (3) self-association (i.e., b + b = 2b).

For the general reaction ib + jd = b_id_j (where i = 1, 2, 3, . . . and j = 1, 2, 3, . . .) the activities of the components B and D are related through Equation 4 in the text; that is, $a_B = X_b/X_b^*$ and $a_D = X_d/X_d^*$. If there is no dissociation in either of the single component systems B or in D, then $X_b^* = X_d^* = 1$, and, from above, $a_B = X_b$ and $a_D = X_d$. The total number of moles in the system, n, can be expressed as $n = n_b + n_d + n_{b_id_j}$, or $n = n_B + n_D - (i + j - 1)\cdot n_{b_id_j}$. The following expression for the activity of component B and mole fraction of species b can be obtained:

$$a_B = X_b = \frac{n_B - i\cdot n_{b_id_j}}{n_B + n_D - (i + j - 1)\cdot n_{b_id_j}} = \frac{X_B - \dfrac{i\cdot n_{b_id_j}}{n_B + n_D}}{1 - \dfrac{(i + j - 1)\cdot n_{b_id_j}}{n_B + n_D}} = \frac{X_B - i\cdot\xi}{1 - (i + j - 1)\cdot\xi}$$

where

$$\xi = \frac{n_{b_id_j}}{n_B + n_D}.$$

A similar expression for the activity of component D can be formulated. The general equilibrium constant thus is

$$K = \frac{\dfrac{n_{b_id_j}}{n_B + n_D - (i + j - 1)\cdot n_{b_id_j}}}{\left[\dfrac{n_B - i\cdot n_{b_id_j}}{n_B + n_D - (i + j - 1)\cdot n_{b_id_j}}\right]^i \cdot \left[\dfrac{n_D - j\cdot n_{b_id_j}}{n_B + n_D - (i + j - 1)\cdot n_{b_id_j}}\right]^j} = \frac{\xi\cdot[1 - (i + j - 1)\cdot\xi]^{(i+j-1)}}{(X_B - i\cdot\xi)^i\cdot(X_D - j\cdot\xi)^j}.$$

Simple association

If i = 1, j = 1, the reaction is b + d = bd and the equilibrium constant becomes

$$K = \frac{\xi\cdot(1 - \xi)}{(X_B - \xi)\cdot(X_D - \xi)}.$$

From the above expressions for the activities of the components,

$$a_B = X_b = \frac{X_B - \xi}{1 - \xi} \rightarrow \gamma_B = \frac{1 - \dfrac{\xi}{X_B}}{1 - \xi} \leq 1$$

and similarly for component D.

For example K = 10, the expression for the equilibrium constant can be used to solve for ξ for any chosen X_D, and the activities of the components obtained from the above expressions. Appendix Figure 1 shows the resulting symmetric negative deviations from ideality (curves i).

Complex association

If i = 2, j = 1, the reaction becomes 2b + d = b_2d, and the equilibrium constant becomes

$$K = \frac{\xi\cdot(1 - 2\cdot\xi)^2}{(X_B - 2\cdot\xi)^2\cdot(X_D - \xi)}.$$

The expressions above for the activites of the components become

$$a_B = X_b = \frac{X_B - 2\cdot\xi}{1 - 2\cdot\xi} \rightarrow \gamma_B = \frac{1 - \dfrac{2\cdot\xi}{X_B}}{1 - 2\cdot\xi} \leq 1$$

and

$$a_D = X_d = \frac{X_D - \xi}{1 - 2\cdot\xi} \rightarrow \gamma_D = \frac{1 - \dfrac{\xi}{X_D}}{1 - 2\cdot\xi}.$$

The a_D shows considerably different behavior from a_B. If X_D = 0.5, γ_D = 1; if X_D < 0.5, γ_D < 1; if X_D > 0.5, γ_D > 1, although $\overline{G}^{ex}$ remains <1. This behavior is shown in Appendix Figure 1 (curves ii).

Self-association

For the case of self-association according to the reaction 2b = bb, X_b is given by

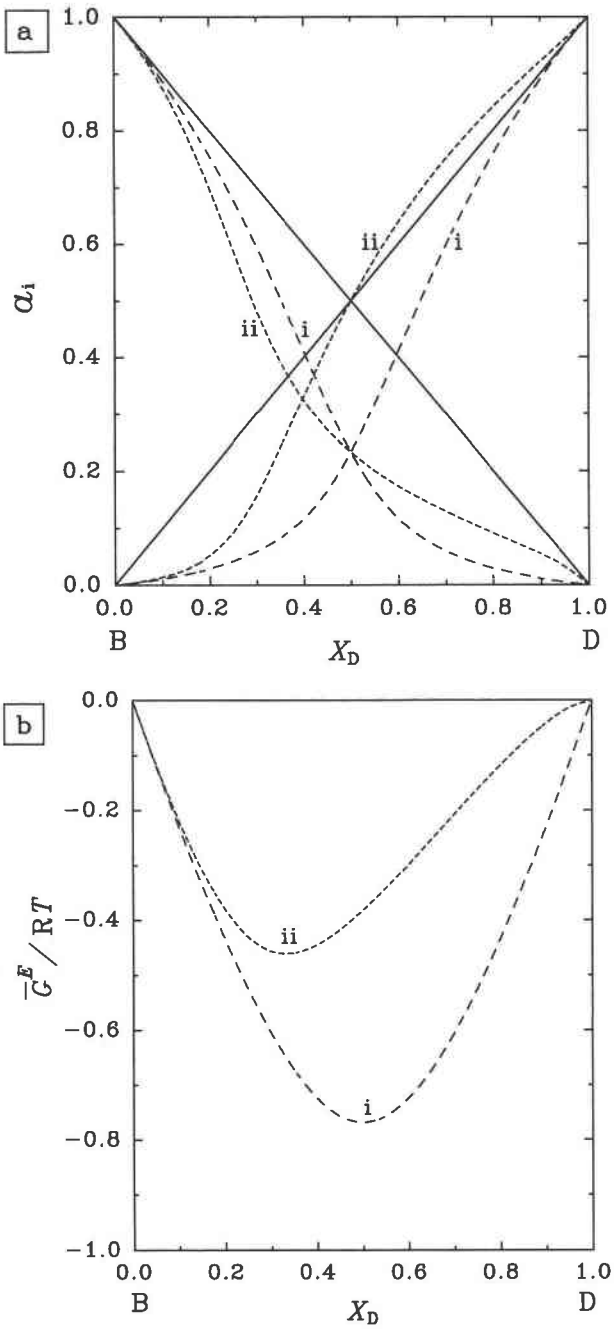

Appendix Fig. 1. (a) Relations between activity and composition and (b) relations between molar excess Gibbs free energy of reaction ($\overline{G}^E$) and composition for the simple association reaction b + d = bd (curves i) and for the complex association reaction 2b + d = b_2d (curves ii) for $K = 10$.

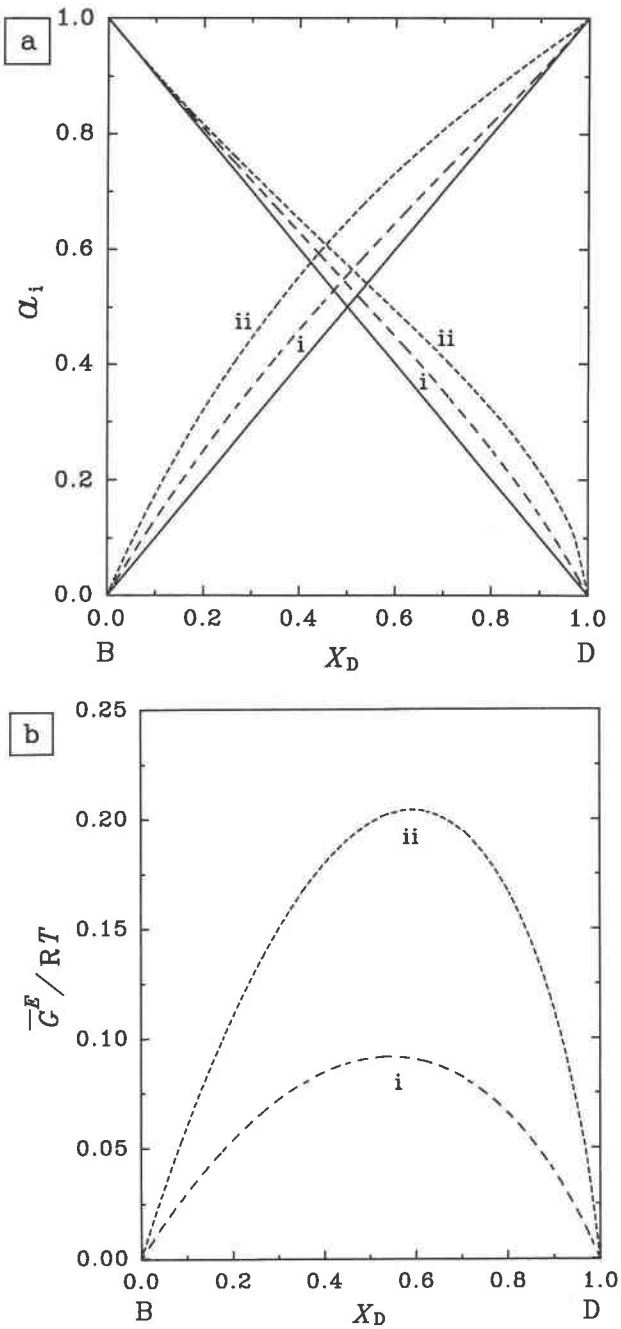

Appendix Fig. 2. (a) Relations between activity and composition and (b) relations between molar excess Gibbs free energy of reaction ($\overline{G}^E$) and composition for the self-association reaction 2b = bb when there is no interaction between b and d species. Curves i are for $K = 1$ and ii for $K = 100$.

$$X_b = \frac{n_B - 2 \cdot n_{bb}}{n_B + n_D - 2 \cdot n_{bb}} = \frac{X_B - 2 \cdot \xi}{1 - \xi}, \quad \text{where} \quad \xi = \frac{n_{bb}}{n_B + n_D}.$$

In this case,

$$X_d = \frac{X_D}{1 - \xi} \quad \text{and} \quad X_{bb} = \frac{\xi}{1 - \xi}.$$

The expression for the equilibrium constant becomes

$$K = \frac{\frac{\xi}{1-\xi}}{\left(\frac{X_B - 2\cdot\xi}{1-\xi}\right)^2} = \frac{\xi - \xi^2}{(X_B - 2\cdot\xi)^2}.$$

Expressing ξ as a function of K,

$$\xi = \frac{4\cdot K\cdot X_B + 1 - \sqrt{1 - 8\cdot K\cdot X_B - (4\cdot K\cdot X_B)^2}}{2(4\cdot K + 1)}.$$

For $X_B = 1$,

$$\xi^* = \frac{1 - \frac{\sqrt{1 - 5\cdot K}}{(4\cdot K + 1)}}{2}, \quad \text{and} \quad X_b^* = \frac{1 - 2\cdot\xi^*}{1 - \xi^*}.$$

For $X_D = 1$, $\xi^* = 0$ and $X_d^* = 1$; therefore,

$$a_B = \frac{X_B - 2\cdot\xi}{1-\xi}\cdot\frac{1-\xi^*}{1-2\cdot\xi^*} \quad \text{and} \quad a_D = \frac{X_D}{(1-\xi)}.$$

Appendix Figure 2 shows the calculated activities and excess molar Gibbs free energies for $K = 1$ (i) and $K = 100$ (ii).